Available online at www.sciencedirect.com
ScienceDirect
Journal of the European Ceramic Society 29 (2009) 669–675
www.elsevier.com/locate/jeurceramsoc

Colloidal processing, hot pressing and characterisation of electroconductive MWCNT-alumina composites with compositions near the percolation threshold

M. Poorteman *, M. Traianidis, G. Bister, F. Cambier

Belgian Ceramic Research Centre, Avenue G. Cornez, B-7000 Mons, Belgium

Received 14 February 2008; received in revised form 9 July 2008; accepted 17 July 2008
Available online 11 September 2008

Abstract

Multiwall Carbon Nanotubes (MWCNT)-alumina nanocomposites have been fabricated by colloidal processing and uniaxial hot pressing.

In the nanotube sols, the electrical conductivity is particularly high, even for low concentrations (≤0.7 vol.%). Classical conductivity models fail to explain this particular behaviour, which is likely to be related to the high aspect ratio of the nanotubes (>70).

Aqueous colloidal processing was performed optimising electrostatic repulsion and conserving the homogeneity by freeze-drying. Inhomogeneities of about 50 μm appeared in the composites and a thermodynamic explanation is suggested based on the free volume of elongated and spherical particles, respectively and considering the persistence length of the nanotubes.

The densification after hot pressing is incomplete (92–93%) even for the low nanotube concentrations considered (<1.4 vol.%).

The composites show electrical conductivity (2.5 S/m) and the percolation threshold is ≤0.6 vol.%.

The conductivity is maintained up to 500 °C in air, degradation of the nanotubes due to oxidation at higher temperatures is likely to occur, decreasing the conductivity.

Keywords: Nanocomposite; Nanotube; Suspension; Persistence length; Electrical conductivity; Al_2O_3

1. Introduction

When electrically conducting particles are dispersed in an electrically isolating matrix, the composite will become conducting at the so called percolation threshold.[1] Indeed, from this concentration limit, a continuous connectivity of the dispersed phase appears in the composite, which in turn becomes conducting. When the dispersed particles are spherical, the critical volume fraction (ϕ_c) above which percolation occurs is 16 vol.%. This value can be largely modified by the geometry of the particles. For instance, the elongated geometry of fibres leads to a high excluded volume, defined as the volume around an object (fibre) into which another similar object is not allowed to enter if overlapping of both objects is to be avoided.[2] If the excluded volume of two conducting fibers overlap, there is a certain probability that they will form a conducting link. Therefore, the critical volume fraction for electrical conductivity decreases as the excluded volume increases.

Carbon nanotubes (CNT) are characterised by a very big length to radius ratio (100 and more). When (semi)-conducting nanotubes are introduced in a poorly conducting ceramic matrix, a much lower percolation threshold can be expected, as shown in the literature.[3,4] However, nanotubes are difficult to process as they have unfavourable geometrical characteristics for colloidal processing,[5] due to a high excluded volume and short interaction distances. As a consequence, they also show electrical conductivity in the sol state for very low nanotube concentrations. However, this is not reflected by any known model up to now as we will show in this paper.

Furthermore, we propose a colloidal processing route, based on electrostatic repulsion between particles, combined with densification by hot pressing in order to study the electrical properties of alumina-MWCNT nanocomposites.

* Corresponding author. Tel.: +32 65 403440; fax: +32 65 348005.
E-mail address: m.poorteman@bcrc.be (M. Poorteman).

0955-2219/$ – see front matter © 2008 Elsevier Ltd. All rights reserved.
doi:10.1016/j.jeurceramsoc.2008.07.047

2. Experimental

Nanocyl®-7000 thin Multiwall Carbon Nanotubes (MWCNT) were used. According to the producer specifications, the nanotubes have an average diameter of about 10 nm and lengths between 0.1 and 10 μm with a mean length of 1.5 μm, as determined from TEM observations. The carbon purity after the Catalytic Chemical Vapour Deposition (CCVD) process is 90%, the remaining impurity being basically encapsulated metal or oxide particles. The surface area specification is between 250 and 300 m^2/g.

Water-based suspensions from Nanocyl, stabilised at pH 4 and with 1 wt.% nanotube content, were used in this study.

As α-alumina raw material, P172SB powder (Alcan Speciality Alumina Europe, Fr; particle size ∼0.4 μm, purity ∼99.7%) was used. An aqueous sol containing 10 wt.% of alumina was prepared at the same pH as that of the nanotube sol.

The grain size distribution of the nanotubes was assessed by laser diffraction granulometry (Malvern Mastersizer). In order to assess the length distribution of the nanotubes, the distribution function, calculated, first, from the diffraction spectrum using a Fraunhofer diffraction model, was recalculated assuming that nanotubes have a fixed diameter of 10 nm.

Mixing of aqueous alumina sols with MWCNT sols (0.6 and 1.4 vol.% nanotubes with respect to the alumina content) was achieved after controlling and optimising the ζ potential and grain size distribution by electroacoustic and attenuation measurements of each sol, respectively (Acoustosizer II, Colloidal Dynamics, USA).

In order to preserve the homogeneity of the mixture, the suspension was rapidly frozen with liquid nitrogen and drying was carried out by freeze-drying.

The dried powder mixtures were densified by uniaxial hot pressing (KCE, Ge) under argon and the shrinkage was followed up by a Linear Variable Displacement Transducer (LVDT). All samples prepared for resistivity measurement were densified at 1450 °C during 30 min under 30 MPa uniaxial load. The final density was measured by Archimedes' method.

The homogeneity of the densified samples was assessed by Scanning Electron Microscope (SEM) observation of gold-coated rupture faces obtained after three point bending tests with a span of 15 mm and a crosshead speed of 0.1 mm/min. The microstructure was further assessed by Field-Effect-Gun Scanning Electron Microscope (FESEM). In order to assess the critical defect size, the critical stress intensity factor (K_{IC}) was measured using the Single Edge Notched Beam (SENB) technique.

Impedance measurements were assessed on plane grinded samples, in order to achieve parallel faces, and after platinum coating of the cylinder faces by sputtering. The resistivity was assessed at 100 Hz, from room temperature up to 550 °C.

3. Results and discussion

3.1. Characterisation of the aqueous nanotube suspension

The grain size distribution of the nanotubes is shown in Fig. 1. Particles have calculated lengths between 0.7 and 10 μm. The mean volume diameter is calculated to be 1.67 μm which is close to the mean value measured by Transmission Electron Microscope (TEM) by the producer (1.5 μm). Considering the particle diameter to be equal to the mean value (10 nm) the length to diameter ratio therefore varies between 70 and 1000.

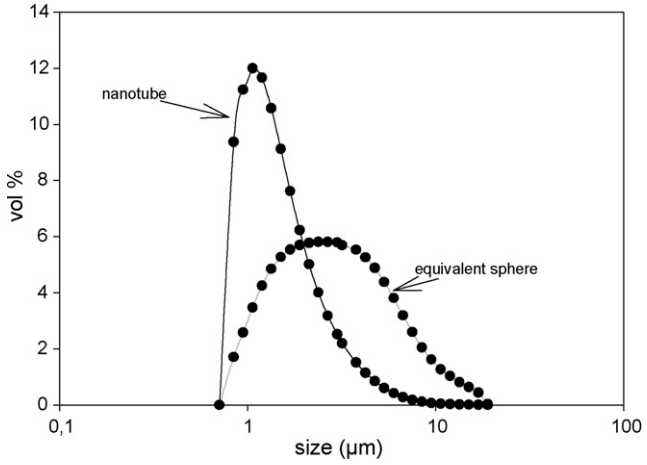

Fig. 1. Calculated length distribution function of the nanotubes.

The ζ potential of the MWCNT sol, calculated from the acoustic response measured by acoustosizer, was −33 mV. The parameters introduced in the model developed by R.W. O'Brien for calculating the complex dynamic mobility[6,7] was a density of 1.4 $g\,cm^{-3}$, obtained from the technical data sheet of the producer, whereas the dielectric constant did not significantly influence the result.

The measured electrical conductivity of the nanotube suspension was 0.8 S/m.

The concentration dependence of the electrical conductivity of the nanotube sol was assessed. In order to measure at constant ionic strength, KCl was added in order to have a fixed background of 0.01 M electrolyte concentration with an intrinsic electrical conductivity $\sigma_0 = 0.12$ S/m.

The electrical conductivity, σ, of the sol increases as the nanotube concentration increases (Fig. 2).

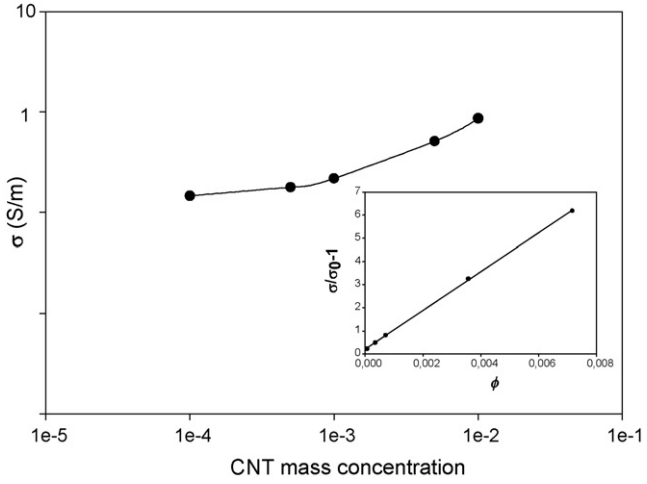

Fig. 2. Concentration dependence of electrical conductivity of the nanotube sol.

The concentration dependence of the electrical conductivity of elongated particles can be described by the Hamilton and Crosser model[8] in order to take into account the non-sphericity of the particles. This model is predicting the following dependence of the sol conductivity σ as a function of the volume fraction ϕ of the dispersed, conductive, phase:

$$\sigma = \sigma_0 \left(1 + \frac{3\phi}{\varepsilon(1-\phi+3/\varepsilon(\alpha-1))}\right) \quad (1)$$

For small concentrations ($\phi \to 0$) and large α, Eq. (1) reduces to:

$$\sigma/\sigma_0 - 1 \approx 3\phi/(\varepsilon + 3/\alpha) \quad (\alpha \gg 1) = \frac{\phi}{\varepsilon/3 + 1/\alpha} \quad (2)$$

$$\sigma/\sigma_0 - 1 \approx \frac{3\phi}{\varepsilon} \quad (\alpha > 70 \text{ and } 0.1 < \varepsilon < 0.3) = n\phi \quad (3)$$

- $\alpha = \sigma_c/\sigma_0$ is the dimensionless ratio of conductivities, where σ_c is the conductivity of the MWCNT particles. It is known to be very high as the conductivity of CNTs is estimated to be of order 1000 S/m.[9] Therefore, $\alpha \sim 10^4$.
- ε is the so called sphericity which is the ratio of the surface area of a spherical particle to the surface area of an elongated particle of equivalent volume. The mean value of ε, $\langle\varepsilon\rangle$, was determined from Fig. 1 and calculated to be 0.25.
- n is a coefficient (the shape factor) equal to 3 in the simplified Maxwell model (spheres) and to $3/\varepsilon$ in the extended model of Hamilton and Crosser.

From Eq. (3) it follows that n should correspond to the slope of Fig. 2, which appears to be 840. However, according to the Hamilton Crosser model, the theoretical slope $\sim 3/\varepsilon$ is about 12, as $\langle\varepsilon\rangle$ is about 0.25. As a consequence, the electrical conductivity of the MWCT sol shows an unexpected behaviour.[5] This kind of behaviour is not explained in the literature, as the model taking into account anisotropy (Hamilton Crosser) does not consider particles with such a high aspect ratio. Due to this high aspect ratio, the excluded volume between nanotubes is also high and as a consequence the number of contacts between (semi)-conducting nanotubes, and therefore the conductivity, is increased.

3.2. Processing of the composites

3.2.1. Mixing of alumina and nanotube suspensions

At pH 4, alumina has a positive ζ potential. In order to avoid attraction between the negatively charged nanotubes and the alumina particles, citric acid was used as a chelating agent to modify the surface charge of the latter from positive to negative.

From Fig. 3 the ζ potential appears to decrease as citric acid is added and after addition of 0.3 wt.% citric acid with respect to the alumina dry matter content the chemisorption limit of citric acid at the alumina surface is reached. As the ζ potential decreases, the grain size, measured by attenuation increases (Fig. 4).

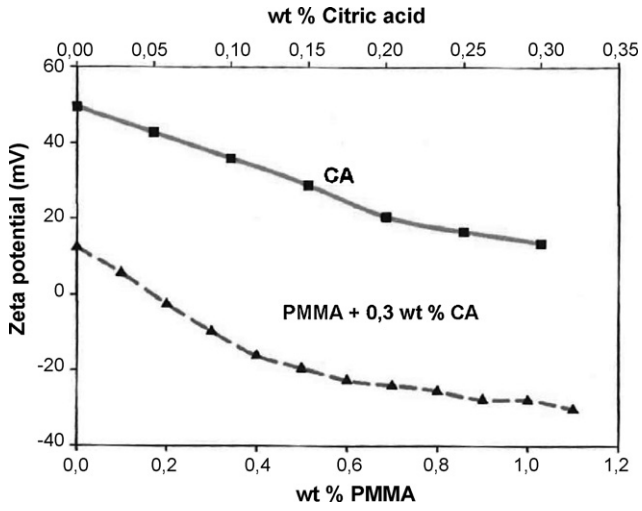

Fig. 3. Influence of sphericity and aspect ratio on the shape factor. Zeta potential of alumina sol at pH 4 and addition of citric acid and consecutive addition of PMMa.

In a second step, an anionic polyelectrolyte dispersant, a polymethylmetacrylic ammonium salt (PMMa), was added in order to further reduce the ζ potential and stabilise the suspension. As the ζ potential progressively becomes more negative, the grain size decreases again (Fig. 4). The optimum adsorption conditions were achieved after addition of 1.1 wt.% PMMa.

After adding the optimum quantity of dispersants, the sol was aged for 60 h and the grain size distribution measured by acoustic attenuation. After readjustment of the pH to 4, the median grain diameter, d_{50}, measured in this way was 0.25 μm and the d_{85} 1.06 μm. The stability of this sol was checked by turbidimetry and no significant sedimentation appeared to have taken place after 24 h testing.

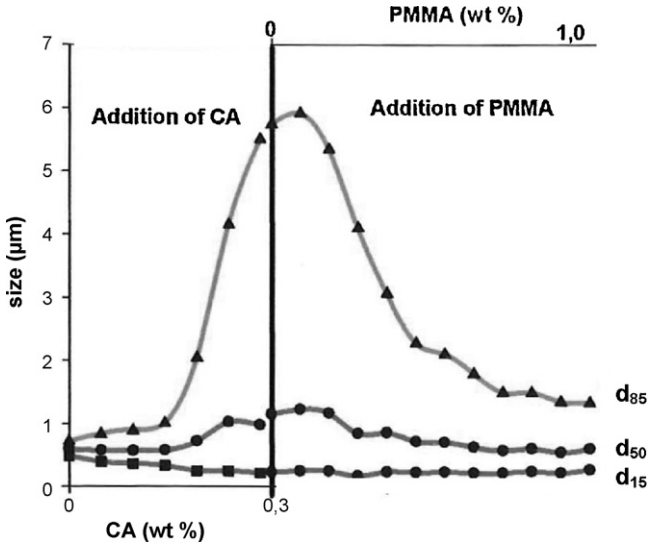

Fig. 4. Grain size of alumina sol at pH 4 and citric acid and PMMa content, respectively.

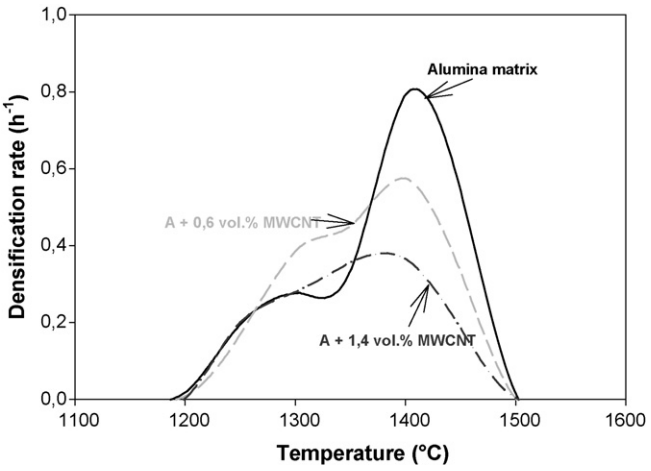

Fig. 5. Temperature dependence of the densification rate and MWCNT content.

3.2.2. *Densification of freeze dried powder mixtures by hot pressing*

The densification of the alumina matrix and the nanocomposites by uniaxial hot pressing showed two densification domains (Fig. 5). A first densification peak occurs around 1300 °C and a second one around 1400 °C. It is well known from the literature[10] that the first peak corresponds to grain rearrangement whereas the second peak corresponds to diffusion-related densification of alumina or a combination of both.

Addition of nanotubes increases the first densification peak whereas it decreases the second one. The first increase in densification rate can be related to a less efficient initial alumina matrix packing in the composite system through the addition of secondary particles with a high aspect ratio.[11] Another explanation is given by Peigney *et al.* who attribute the increased grain rearrangement to the fact that CNTs facilitate sliding at grain contacts and therefore to a lower friction coefficient between grains.[12] As a consequence the grain rearrangement densification mechanism will be increased. The second decrease in densification rate can be related to the formation of a rigid network of MWCNT providing a sintering constraint.[13] Indeed, as shown in the electrical measurement part (Section 3.3.2), percolation of nanotubes is likely to occur in the studied compositions confirming the above hypothesis. Other authors attribute the decrease in shrinkage in the longitudinal direction to a decrease in shear stresses in the longitudinal direction, redistributing the stresses in the transversal direction, and therefore inhibiting plastic flow.[12]

Hot pressing of alumina-CNT nanocomposites has been studied by several authors.[14–16] It is not easy to compare the results of this study with those found in literature as

- The characteristics of the nanotubes sometimes lack or are completely different than those used in the present study, where the nanotubes are particularly long;
- the processing is completely different (in situ synthesis, coating of nanotubes with matrix particles) and therefore the obtained nanocomposite has different characteristics;

Table 1
Density characteristics of hot-pressed samples

MWCNT (wt.%)	0	0.2	0.5
MWCNT (vol.%)	0	0.6	1.4
Bulk density	3.94	3.68	3.60
Theoretical density (%)	99.0	93.3	91.7
Open porosity (vol.%)	0.3	0.6	3.1

- the use of catalyst interferes with the densification mechanism, for instance the catalyst content changes the densification characteristics;
- the characteristics of the alumina matrix sometimes appear to be completely different (use of nanometric alumina).

The end material can therefore be completely different depending on the raw material characteristics (kind of alumina matrix and CNT, presence of encapsulated metal or oxide particles).

As a consequence, densified nanocomposites with an alumina matrix can sometimes have lower and sometimes higher densities than the corresponding monolithic material.

All composites have been densified at the maximum densification rate, which is at about 1450 °C.

The final density obtained after hot pressing at 1450 °C during half an hour at 30 MPa is presented in Table 1.

Although the volume of added nanotubes in the composites is rather low, their impact on the final density is rather high and severely reduces the final density and increases the open porosity.

3.3. *Characterisation of hot-pressed samples*

3.3.1. *Homogeneity of hot-pressed samples*

SEM analysis of rupture faces showed dark zones to appear at or near the fracture origin, corresponding to the presence of light elements (Fig. 6). Comparing Energy Dispersive X-ray (EDX) analysis inside and outside this zone shows that dark zones are characterised by a low alumina and high carbon content. Therefore it is likely to correlate these observations with the presence of nanotube agglomerates. The size of this

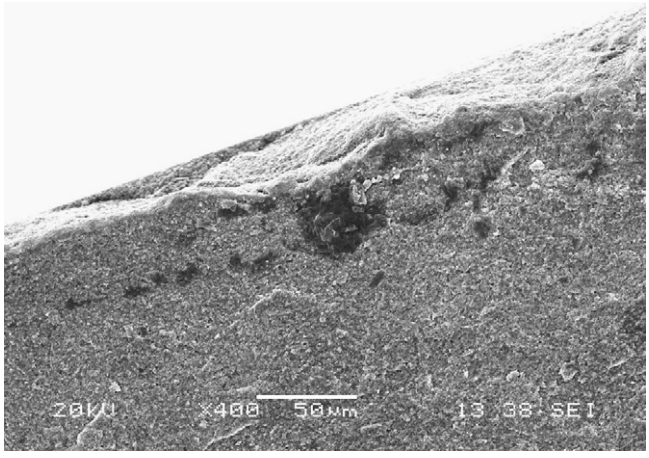

Fig. 6. SEM analysis of rupture faces of nanocomposites (fracture origin).

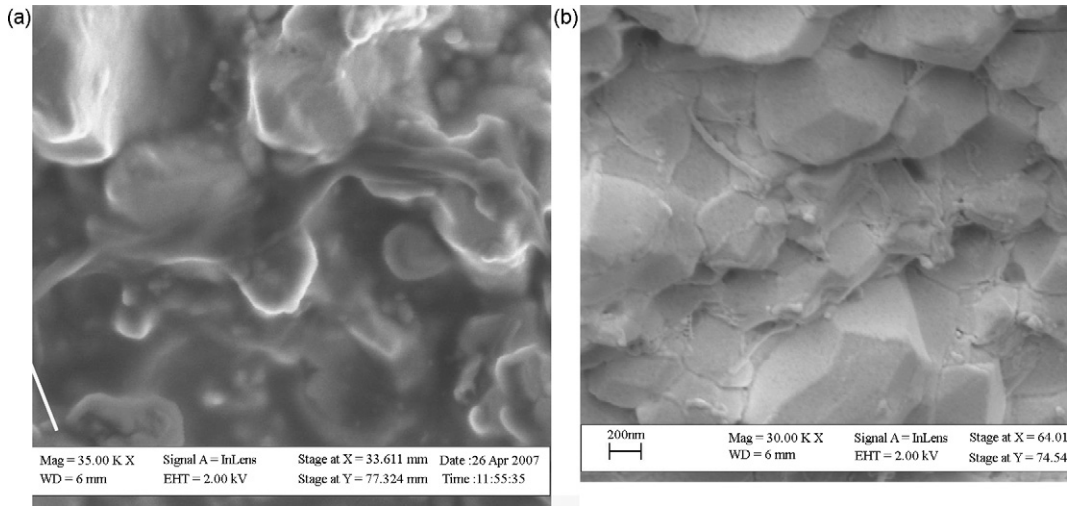

Fig. 7. FESEM analysis of nanocomposites containing 0.6 vol.% nanotubes. (a) FESEM inside dark zone. The arrow shows a nanotube rope. (b) FESEM outside dark zone.

agglomerated zone can reach 50 μm. This size is close to the critical defect size (60 μm) calculated from Griffith's equation for a measured flexural strength of 373 ± 63 MPa and a K_{IC} value of 3.7 ± 0.3 MPa $\sqrt{m}$.

It was possible to identify bundled nanotubes inside the dark zone (Fig. 7a) by FESEM, whereas outside those zones, percolating nanotube structures could be identified (Fig. 7b).

In spite of all the precautions undertaken to establish a high degree of homogeneity in both the nanotube and alumina sols individually and during mixing by favouring electrostatic repulsion, the samples hot pressed from the freeze dried powder mixtures show a remarkable degree of inhomogeneity. Indeed, large (up to 50 μm) carbon rich zones containing bundled nanotubes can be identified at the fracture origin.

Some authors have attributed this tendency of forming agglomerates to Van der Waals attractive interactions between nanotubes.[17] Although such kind of attractive forces definitely exist in the systems under study, they are not expected to lead to such important inhomogeneities, considering the high stability (high magnitude of ζ potential) and compatibility (same repulsive forces in both cases) of both sols. Moreover, the nanotube content is rather low.

Instead, we suggest that other forces might play a key role in the behaviour of the mixtures we have studied. Indeed, it has been shown from thermodynamic considerations,[18] based on an extension of the free volume method,[19] and also by numerical simulation of mixtures of hard spheres and thin rodlike polymers of varying length,[20] that long, thin rods mixed with spheres can induce phase separation. Lekkerkerker *et al.* introduce a characteristic volume fraction of rods, ϕ_c, required to introduce this phase separation. This critical volume scales with $2r/(a_r D)$, with D the diameter of the spherical particles (alumina in this case) and a_r, the aspect ratio, is the ratio of the length (h) to the diameter ($2r$) of the nanotubes.

It follows that for rods with high aspect ratio and a small diameter, very low volume fractions of rods are needed to induce phase separation. Although these results are restricted to $h/D \leq 1$, these conditions are satisfied by a part of the nanotubes since their length decreases below 1 μm and spheres with sizes above 1 μm also exist ($d_{85} > 1$ μm). We also assimilate the nanotubes with rods, which is, at first sight, another approximation. However, the nanotubes are likely to have a high aspect ratio in the sol state because this explains the very high electrical conductivity observed in the nanotube suspension. Moreover, the stiffness of a CNT can be evaluated by a concept from polymer science: the persistence length. The persistence length is defined as the length over which correlations in the direction of the tangent are lost. If we define the angle ϑ between a vector that is tangent to the polymer at position 0 and a tangent vector at distance L away from position 0 it can be shown that the expectation value of the cosine of the angle falls of exponentially with distance,

$$\langle \cos \vartheta = e^{-(L/P)} \rangle$$

where P is the persistence length and $\langle\ \rangle$ corresponds to the average over all starting positions.

Pieces of the polymer that are shorter than the persistence length behave rather like a flexible elastic rod, while properties are described by a random walk in the other case (the persistence length of cooked spaghetti is about 10 cm, whereas for DNA it is about 50 nm). It has been shown in the literature that the dynamic persistence lengths, i.e. considering the thermal energy in Brownian motion, of CNT are expected to be in the order of tens to hundreds of micrometers, and nanotubes should therefore behave like short, stiff carbon fibres.[21]

Under these conditions ($h/D \leq 1$, and stiff nanotubes), theoretical prediction gives values of ϕ_c around 0.5 vol.% which is close to the values used in this work and which might explain the occurrence of extended agglomerates.

The numerical study of the phase diagram of a mixture of spherical and rodlike colloids by Bolhuis *et al.* does not make any other assumption concerning the rodlike needles except than considering them infinitely thin, which appears to be a good approximation for the very thin nanotubes. The authors obtain

Table 2
Electrical resistivity and nanotube content

Material	Resistivity (Ω cm)
Alumina matrix	7.7×10^{11}
Composite with 0.2 wt.% nanotubes	484.0
Composite with 0.5 wt.% nanotubes	39.9

binodal curves leading to a phase separation attributed to a pure entropic effect: the phase separation is caused by an increase in the available volume for the needles as the spheres cluster. As a consequence a dense, hard-sphere rich phase and a dilute phase with few hard spheres are obtained, which again explains the observed inhomogeneity.

3.3.2. Electrical measurements

α-Alumina is electrically isolating and has a very high resistivity. A room temperature resistivity of 7.7×10^{11} Ω cm. was measured. The addition of small quantities of MWCNT leads to a decrease of the resistivity of order 8–9, depending on the nanotube concentration (Table 2).

The percolation threshold of the nanotubes in the alumina matrix should therefore be below 0.6 vol.%. These values are comparable with those found in the literature for polymer and ceramic matrix CNT nanocomposites (below 1 vol.%).[3,4,22]

The high temperature resistivity measurements in air are shown in Fig. 8. We observe, first, a slight decrease of the resistivity. From about 380 °C, the resistivity gradually increases for temperatures up to about 500 °C, from which temperature it increases very rapidly. This behaviour can be explained by Differential Scanning Calorimetry (DSC) data found in the literature.[23] Indeed, it has been shown that in this temperature field (380–500 °C) two exothermal phenomena occur for CNT synthesized by CCVD:

- A first oxidation peak at 380 °C, with a mass loss. TEM observation has shown that well structured MWCNT were present at that temperature, the nanotubes with defaults having disappeared,

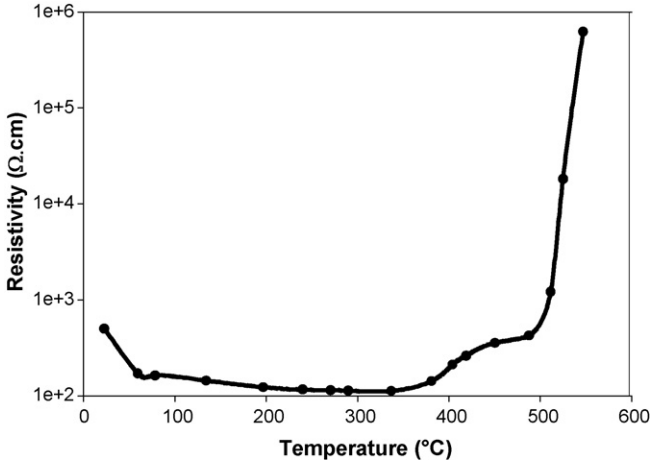

Fig. 8. Electrical resistivity and conductivity of 0.2 wt.% nanocomposite as a function of temperature.

- a second oxidation peak at 500 °C, also with a mass loss. TEM observation has shown that the MWCNT had shortened at that temperature.

These observations corroborate the high temperature electrical behaviour of the CNT composites. It has been shown in the literature that the presence of defects in nanotube structures interferes with the electrical properties. Indeed, heterojunctions can introduce potential steps leading to a semiconducting barrier decreasing the global conductivity.[24] The disappearance of those nanotubes from 380 °C has therefore a lower impact on the global conductivity compared to the influence of the oxidation of better structured MWCNT which occurs from 500 °C. The latter are progressively shortened, leading to less continuous electrical pathways through the material and therefore to a severe reduction of the conductivity.

4. Conclusions

Aqueous CNT sols appear to be stable only for very low concentrations ($\phi \leq 0.7$ vol.%). In this concentration field, the nanotubes highly contribute to the electrical conductivity of the sol, due to their intrinsic conductivity and to their high aspect ratio, a_r.

The nanotube sol, having a negative ζ potential, was mixed with a stabilised alumina sol having the same sign of ζ potential in order to favour stabilisation of the mixture through electrostatic repulsion.

After freeze-drying, in order to retain the obtained homogeneity, the powder mixtures were densified by uniaxial hot pressing. The attained final density varied between 92 and 93% for the compositions studied (0.6 and 1.4 vol.% of nanotubes). Nanotubes appear to decrease the packing density of the powder mixtures and also hinder the second stage densification probably by formation of a rigid network.

The microstructure is characterised by percolating structures on the one side, but on the other side also by carbon rich clusters up to 50 μm assimilated with nanotubes. The reason invoked for this inhomogeneity is based upon demixtion of isotropic particles and particles with a high aspect ratio. Demixtion is able to occur because of the high excluded volume of the nanotubes.

The densified composites show electrical conductivity (as high as 2.5 S/m) from a volume fraction of 0.6 vol.%, which is likely to be an upper limit for percolation.

The conductivity is maintained in air up to temperatures as high as 500 °C, at higher temperatures, the nanotubes are probably damaged and the conductivity decreases rapidly.

Acknowledgments

Appreciation is expressed to Dr. Alain Stroobants (formerly University of Utrecht) and Dr. Fabrice Petit (BCRC) for their helpful discussions, Dr. Christophe Pirlot from Nanocyl (B) for the technical data on nanotubes and to Prof. Pascal Jacques from UCL (B) for the FESEM observations. The onset of our research was induced by the Ceratex project sponsored by IWT (B).

References

1. McLachlan, D. S., Blaszkiewicz, M. and Newnham, R. E., Electrical resistivity of composites. *J. Am. Ceram. Soc.*, 1990, **73**(8), 2187–2203.
2. Balberg, I., Anderson, C. H., Alexander, S. and Wagner, N., Excluded volume and its relation to the onset of percolation. *Phys. Rev. B: Condens. Mater.*, 1984, **B30**, 3933–3943.
3. Rul, S., Lefèvre-schlick, F., Capria, E., Laurent, Ch. and Peigney, A., Percolation of single-walled carbon nanotubes in ceramic matrix nanocomposites. *Acta Mater.*, 2004, **52**, 1061–1067.
4. Hu, L., Hecht, D. S. and Grüner, G., Percolation in transparent and conducting carbon nanotube networks. *Nano Lett.*, 2004, **4**(12), 2513–2517.
5. Sun, J., Gao, L. and Li, W., Colloidal processing of carbon nanotube/alumina composites. *Chem. Mater.*, 2002, **14**, 5169–5172.
6. Greenwood, R., Review of the measurement of zeta potentials in concentrated aqueous suspensions using electroacoustics. *Adv. Colloid Interface Sci.*, 2003, **106**(1–3), 55–81.
7. O'Brien, R. W., Jones, A. and Rowlands, W. N., A new formula for the dynamic mobility in a concentrated colloid. *Colloids Surf. A: Physicochem. Eng. Aspects*, 2003, **218**, 89–101.
8. Hamilton, R. L. and Crosser, O. K., Thermal conductivity of heterogeneous two-component systems. *I & EC Fundamentals*, 1962, **1**(3), 187–191.
9. Ebbesen, T. W., Lezec, H. J., Hiura, H., Bennett, J. W., Ghaemi, H. F. and Thio, T., Electrical conductivity of individual carbon nanotubes. *Nature*, 1996, **382**(4), 54–56.
10. Coble, R. L. and Ellis, J. S., Hot-pressing alumina, mechanisms of material transport. *J. Am. Ceram. Soc.*, 1963, **46**(9), 438–441.
11. Poorteman, M., Descamps, P., Cambier, F. and Leriche, A., Hot isostatic pressing of SiC-platelets/Y-TZP composites. *J. Eur. Ceram. Soc.*, 1993, **12**, 103–109.
12. Peigney, A., Rul, S., Lefèvre-Schlick, F. and Laurent, C., Densification during hot-pressing of carbon nanotube-metal-magnesium aluminate spinel nanocomposites. *J. Eur. Ceram Soc.*, 2007, **27**, 2183–2193.
13. Lange, F. F., Constrained Network Model for predicting densification behaviour of composite powders. *J. Mater. Res.*, 1987, **2**(1), 59–65.
14. Laurent, Ch., Peigney, A., Dumortier, O. and Rousset, A., Carbon nanotubes-Fe-alumina nanocomposites. Part II: microstructure and mechanical properties of the hot-pressed composites. *J. Eur. Ceram. Soc.*, 1998, **18**, 2005–2013.
15. Fan, J., Zhao, D., Wu, M., Xu, Z. and Song, S., Preparation and microstructure of multi-wall carbon nanotubes-toughened Al_2O_3 composite. *J. Am. Ceram. Soc.*, 2006, **89**(2), 750–753.
16. Wei, T., Fan, Z., Luo, G. and Wie, F., A new structure for multi-walled carbon nanotubes reinforced alumina nanocomposite with high strength and toughness. *Mater. Lett.*, 2008, **62**, 641–644.
17. Lisunova, M. O., Lebovka, N. I., Melezhyk, O. V. and Boiko, Y. P., Stability of the aqueous suspensions of nanotubes in the presence of nonionic surfactant. *J. Colloid Interface Sci.*, 2006, **299**, 740–746.
18. Vliegenthart, G. A. and Lekkerkerker, H. N. W., Phase behaviour of colloidal rod-sphere mixtures. *J. Chem. Phys.*, 1999, **111**(9), 4153–4157.
19. Lekkerkerker, H. N. W. and Stroobants, A., On the spinodal instability of highly asymmetric hard sphere suspensions. *Phys. A*, 1993, **195**, 387.
20. Bolhuis, P. and Frenkel, D., Numerical study of the phase diagram of a mixture of spherical and rodlike colloids. *J. Chem. Phys.*, 1994, **101**(11), 9869–9875.
21. Lee, H. S., Yun, C. H., Kim, H. M. and Lee, C. J., Persistence length of multiwalled carbon nanotubes with static bending. *J. Phys. Chem. C*, 2007, **111**, 18882–18887.
22. Sandler, J. K. W., Kirk, J. E., Kinloch, I. A., Shaffer, M. S. P. and Windle, A. H., Ultra-low percolation threshold in carbon-nanotube-epoxy composites. *Polymer*, 2003, **44**(19), 5893–5899.
23. G. Bister, *Etude de la synhèse par CCVD et du mécanisme de formation des nanotubes de carbone monoparois*, PhD thesis, Facultés Universitaires Notre-Dame de la Paix (Namur, B), 2005, 112–115.
24. Zao, Z., Postma, H. Ch., Balents, L. and Dekker, C., Carbon nanotube intramolecular junctions. *Nature*, 1999, **402**, 273.